Supplementary information

Robust Vibrational Coherence Protected by Core-Shell Structure in Silver Nanoclusters

Jie Kong,[1#] Zhuoran Kuang,[2#] Wei Zhang,[1#] Yongbo Song,[3] Guo Yao,[4] Chunfeng Zhang,[4] He Wang,[5] Yi Luo,[1*] Meng Zhou[1*]*

[1]Hefei National Research Center for Physical Sciences at the Microscale, University of Science and Technology of China, Hefei, Anhui 230026, P. R. China

[2]State Key Laboratory of Information Photonic and Optical Communications, School of Science Beijing University of Posts and Telecommunications (BUPT), Beijing 100876, P. R. China

[3]School of Biomedical Engineering, Research and Engineering Center of Biomedical Materials, Anhui Medical University, Hefei, Anhui 230032, P. R. China

[4]National Laboratory of Solid State Microstructures, School of Physics, and Collaborative Innovation Center for [5]Advanced Microstructures, Nanjing University, Nanjing 210093, P. R. China

[5]Department of Physics, University of Miami, Coral Gables, Florida 33146, United States

[#]These authors contributed equally

*Corresponding author. Email: ybsong860@ahmu.edu.cn; yiluo@ustc.edu.cn; mzhou88@ustc.edu.cn

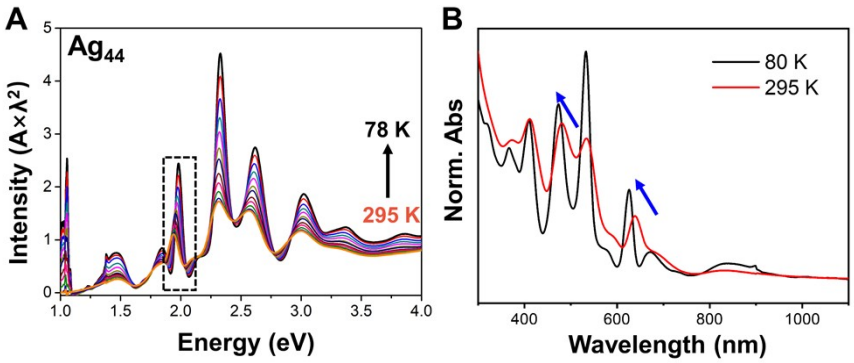

Figure S1. (A) Temperature dependent electronic absorption spectra of Ag_{44} NCs in energy scale. The spike around 900 nm (1.37 eV) is an instrument artifact and the peak around 1.0 eV is the residual absorption of the solvent. (B) The selected temperature dependent normalized (at 400 nm) absorption spectra to show the blue shift.

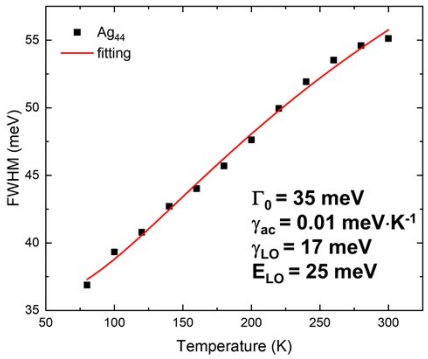

Figure S2. The relationship between the FWHM and temperature for Ag_{44} NCs. The red line is the fitting results according to equation S1.

The tempreture dependent FWHM reflects the vibronic coupling accoud to equation S1,

$$\Gamma(T) = \Gamma(0) + \gamma_{ac}T + \frac{\gamma_{LO}}{e^{E_{LO}/k_B T} - 1} \quad \text{(S1)}$$

where the Γ is the FWHM in eV unit, Γ_0 is the FWHM at 0 K, γ_{ac} and γ_{LO} are the coupling strength to the acoustic phonon and longitudinal optical phonon, E_{LO} is the optical phonon energy.

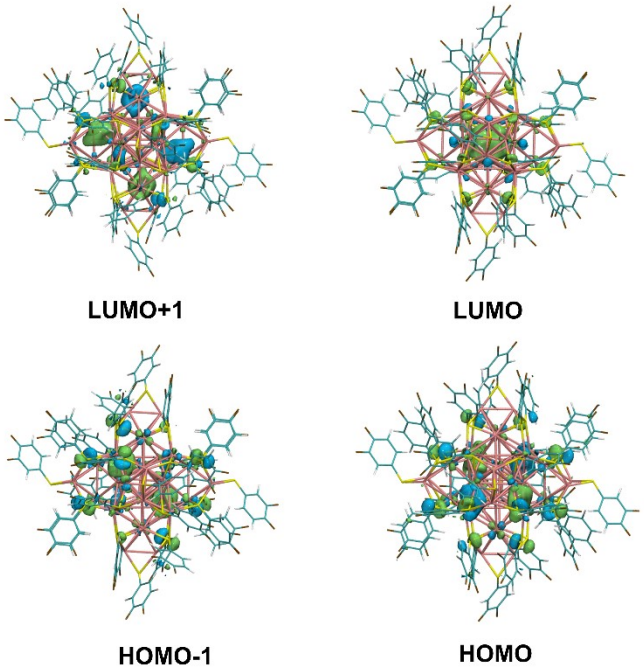

Figure S3. The isosurface of the HOMO-1, HOMO, LUMO, LUMO+1 of Ag_{44} via VMD software. [1]

Table S1. Computed electronic excitation properties for Ag_{44} at the optimized S_0 geometry at the PBEPBE level.

S_0 geometry	$S_0 \rightarrow S_1$	$S_0 \rightarrow S_2$	$S_0 \rightarrow S_3$
E(eV)	0.899	0.932	0.986
Oscillator strength	0	0	0.0054
Main orbital contribution	HOMO→LUMO 98%	HOMO-1→LUMO 98%	HOMO→LUMO+1 94%

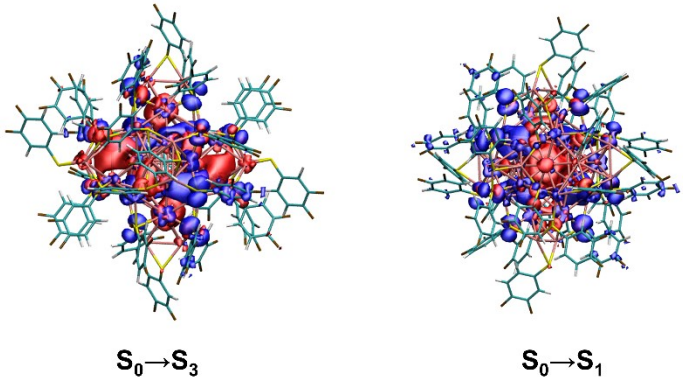

Figure S4. CDDs between $S_{1/3}$ and S_0 states of Ag_{44} at optimized S_0 geometries (The red

and blue represent the electron and hole distributions, respectively).

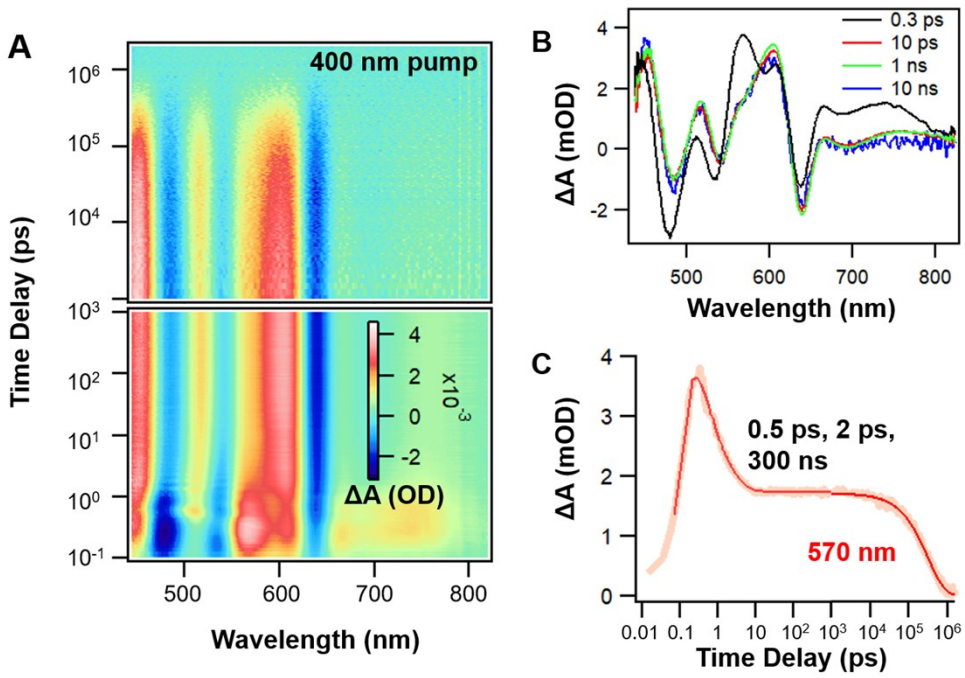

Figure S5. (A) Transient absorption (TA) data map of Ag_{44} with excitation at 400 nm; (B) TA spectra of Ag_{44} at selected time delays; (C) TA kinetic trace probed at 570 nm and the corresponding fit.

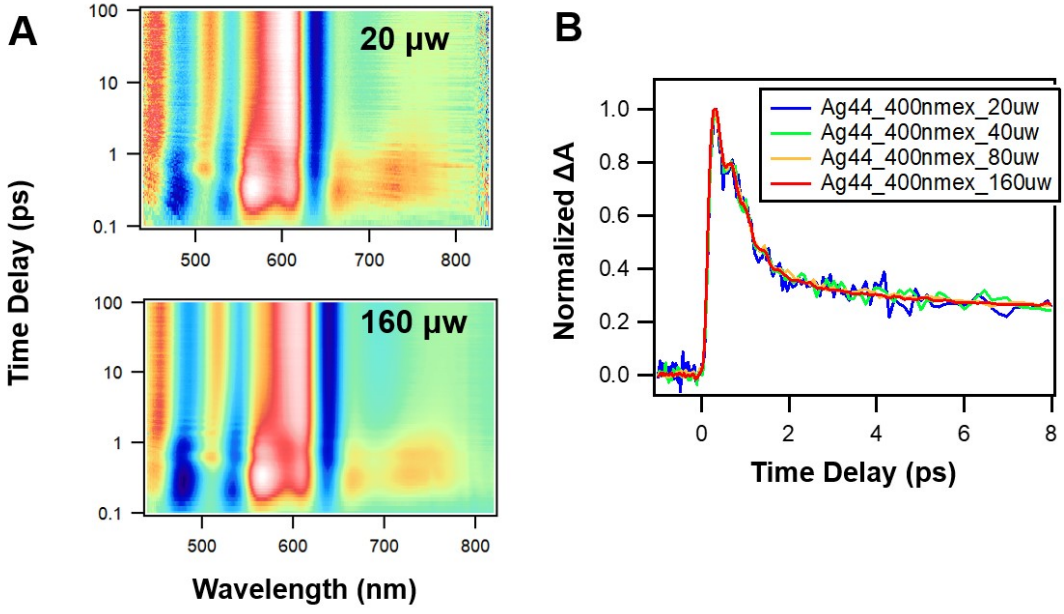

Figure S6. (A) Transient absorption data map of Ag_{44} dissolved in acetone with under different pump power (20 and 160 μw); (B) TA kinetics probed at 670 nm with different pump powers.

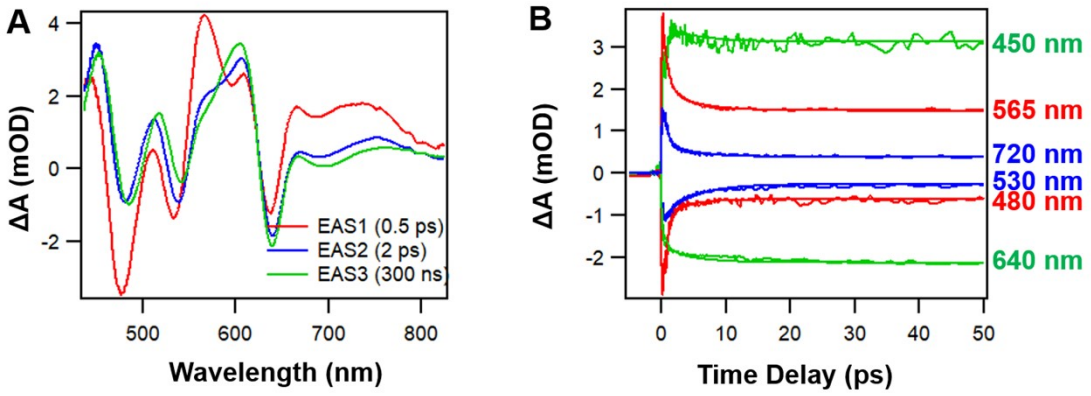

Figure S7. (A) Evolution associated spectra (EAS) obtained from global fitting on the TA data of Ag_{44} pumped at 400 nm; (B) TA kinetics probe at selected wavelengths and the global fitting results.

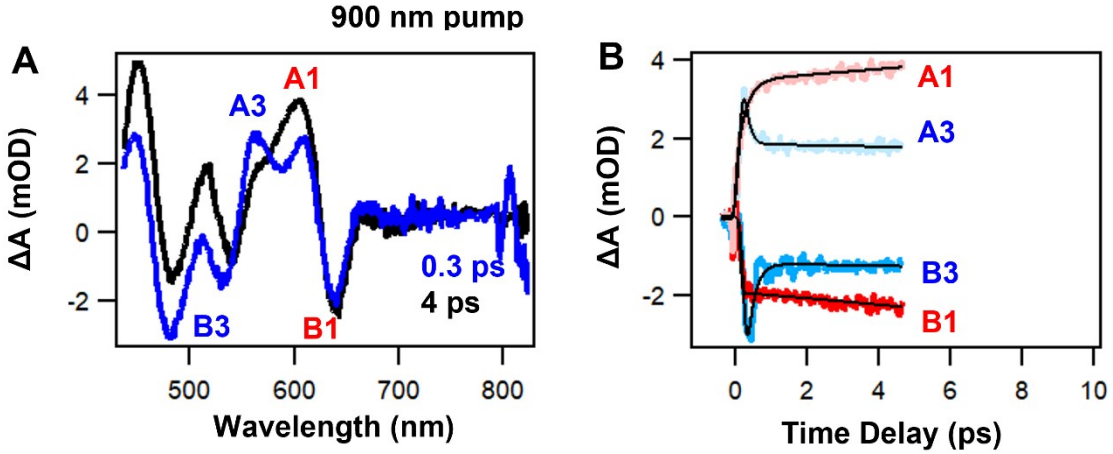

Figure S8 (A) TA spectra probe at 0.3 ps and 4 ps after pumped at 900 nm; (B) TA kinetics probe at selected wavelengths and corresponding fits.

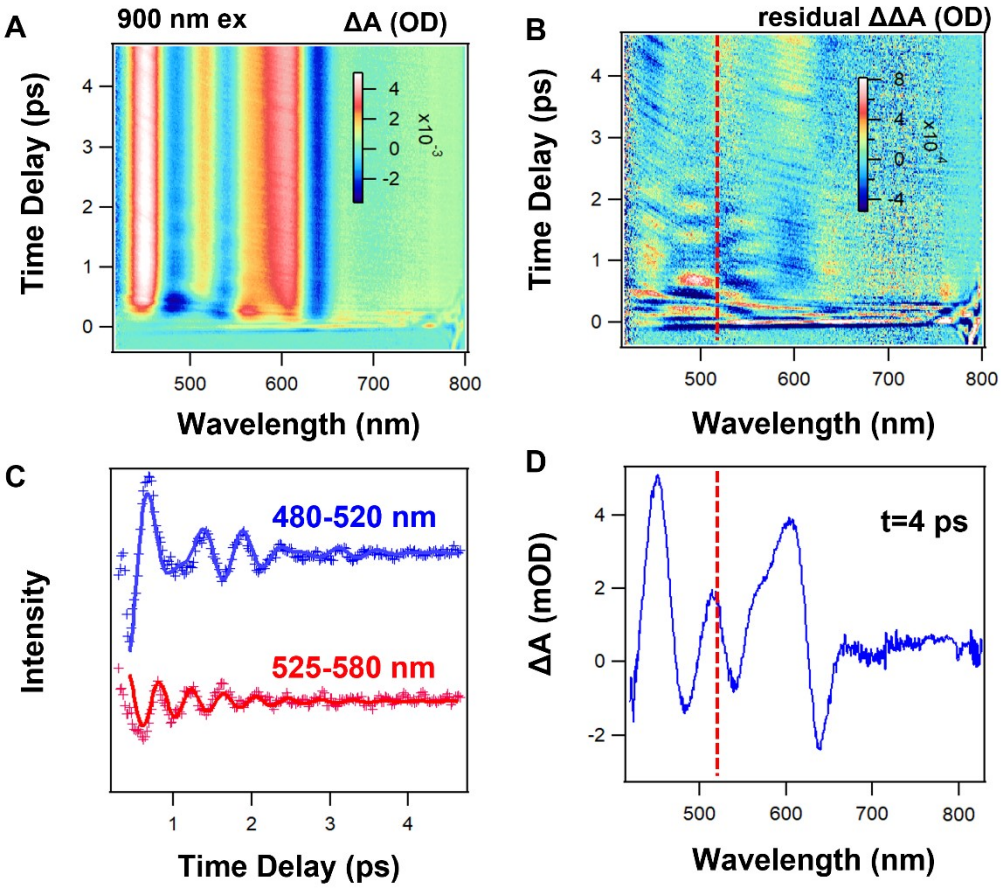

Figure S9. (A) Transient absorption data map of Ag_{44} with 900 nm excitation; (B) TA data map after subtracting population kinetics obtained from global fitting. (C) TA residuals as a function of time delay of Ag_{44} NCs probe at selected wavelength regions and corresponding fits. (D) TA spectrum of Ag_{44} probed at 4 ps, the red dashed line indicates

the probe wavelength where the phase shift occurs.

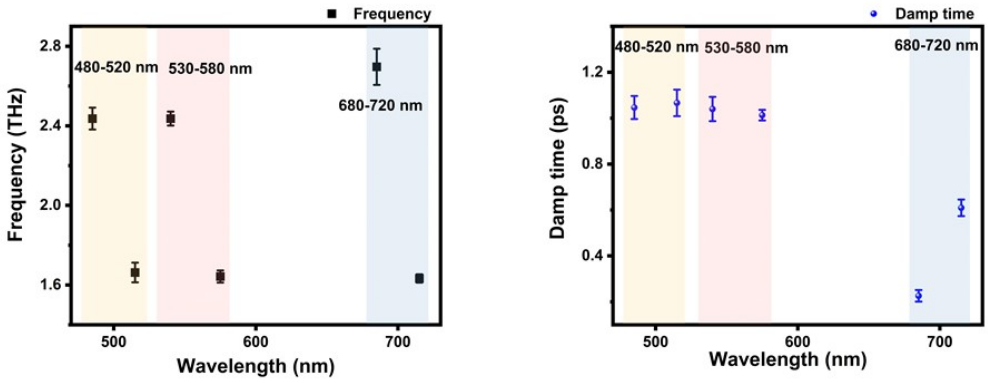

Figure S10. The coherent oscillation results obtained from the fitting results of residual data of Ag_{44} with 400 nm excitation. Note that the error bars were calculated based on three times TA experiments.

Table S2. The coherent oscillation results for Ag_{44} obtained from the fitting results of residual data with 900 nm excitation.

Probe range (nm)	Period (ps)	Frequency (THz)	t_{damp} (ps)
480-520	0.42	2.38	1.0
	0.61	1.67	1.0
525-580	0.41	2.43	1.1

To extract the damping time (τ) of the coherent process, we use a fitting procedure that accounts for the convolution of the Gaussian impulsive function (with standard deviation σ) with the residual decay amplitude and a single or two frequency damped oscillator: [2]

$$f(t) = f_{osc}(t) \int_{-\infty}^{\infty} f_{IRF}(\tau) f_{damp}(t-\tau) d\tau \quad \text{(eq S2)}$$

where

$$f_{osc}(t) = \cos\left(\frac{2\pi}{t_{osc}} t + \varphi\right) \quad \text{(eq S3)}$$

$$f_{damp}(t) = Ae^{-\frac{t}{t_d}} \quad \text{(eq S4)}$$

$$f_{IRF}(t) = \frac{1}{\sqrt{2\pi}w} e^{-\frac{(t-t_c)^2}{2w^2}} \quad \text{(eq S5)}$$

$f_{osc}(t)$ represents the cosine oscillating term, $f_{damp}(t)$ represents the damping term, and $f_{IRF}(t)$ represents the instrumental response function (IRF). The form of convolution can be rewritten as：

$$f(t) = \sum A_i e^{\frac{1}{2}(\frac{w}{t_{di}})^2 - \frac{t-t_c}{t_{di}}} \cos\left(\frac{2\pi}{t_{oscii}}t + \varphi_i\right) \int_{-\infty}^{z} \frac{1}{\sqrt{2\pi}} e^{-\frac{y^2}{2}} dy \quad \text{(eq S6)}$$

in which A_i denotes the amplitude of the *i*th oscillation component, t_{osci} denotes the time constant of the *i*th oscillation component, t_{di} denotes the time constant of the *i*th damping, t_c denotes the time zero of the IRF, $w = FWHM/2\sqrt{ln4}$ and FWHM denotes the full-width-half-maximum of the IRF, φ_i is the relative phase of the *i*th oscillation component, and $z = \frac{t-t_c}{w} - \frac{w}{t_d}$.

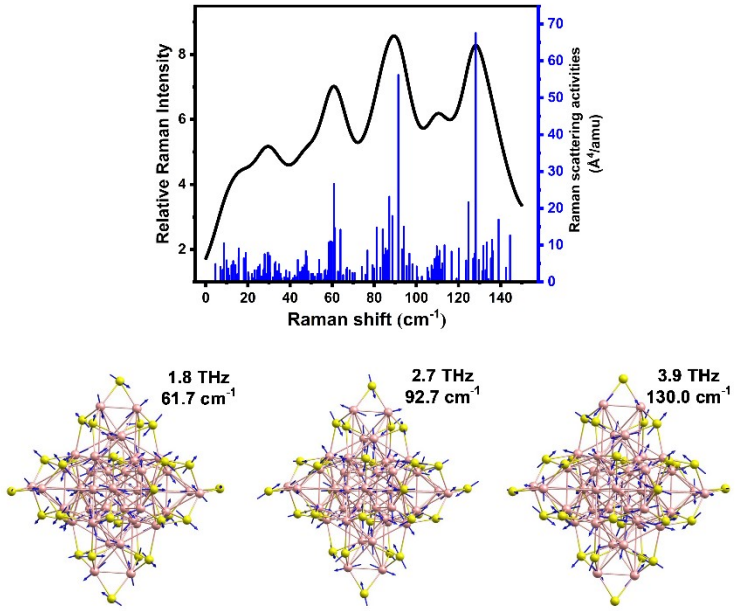

Figure S11. Computed simulation Raman spectra of the Ag_{44} nanocluster (frequency correction factor: 0.986). [3-4]The displacement of selected atoms (arrows), and the vibration modes deduced by DFT computations on Ag_{44}.

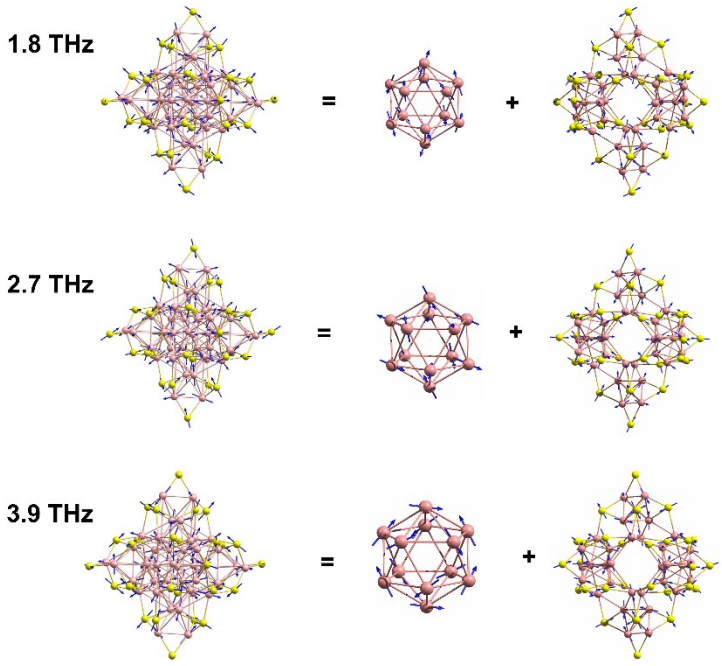

Figure S12. Decomposition of the normal mode of Ag_{44} into contributions from the Ag_{12} core and the $Ag_{32}S_{30}$ ligand binding motifs.

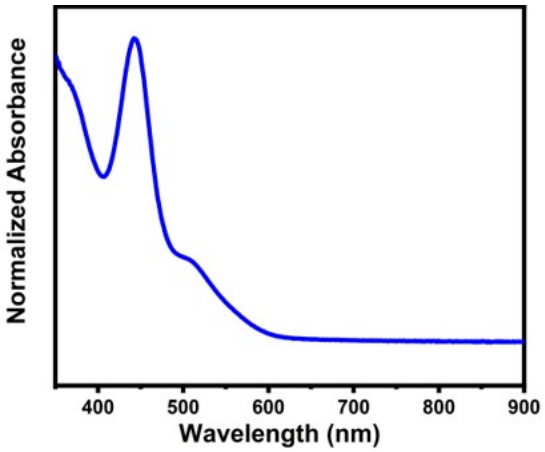

Figure S13. UV-vis absorption spectrum of Ag_{29} NCs.

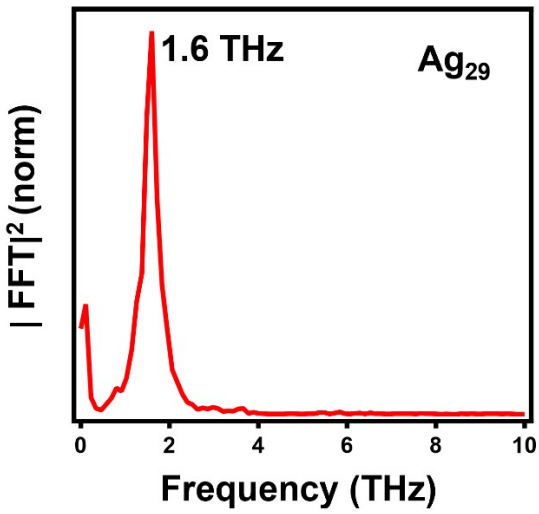

Figure S14. FFT intensity of TA residual of Ag_{29} probed at 550 nm.

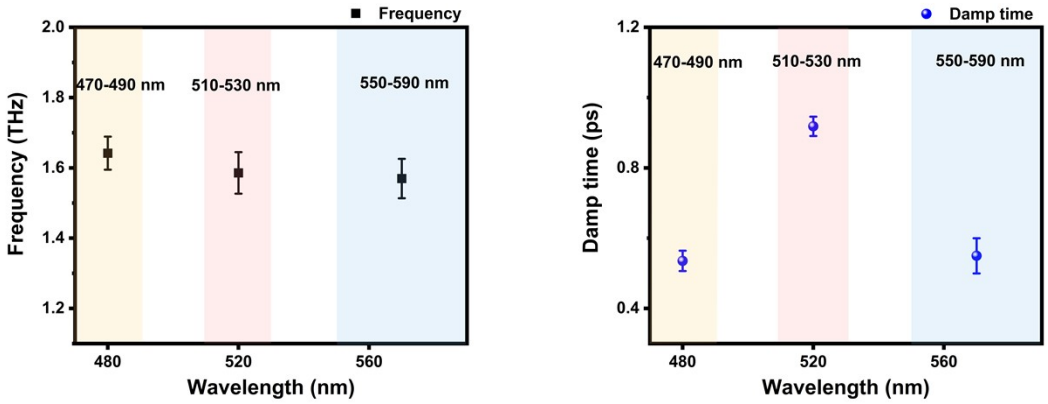

Figure S15. The oscillation frequencies and damp time of Ag_{29} as a function of probe wavelength at 400 nm excitation. Note that the error bars were calculated based on three times TA experiments.

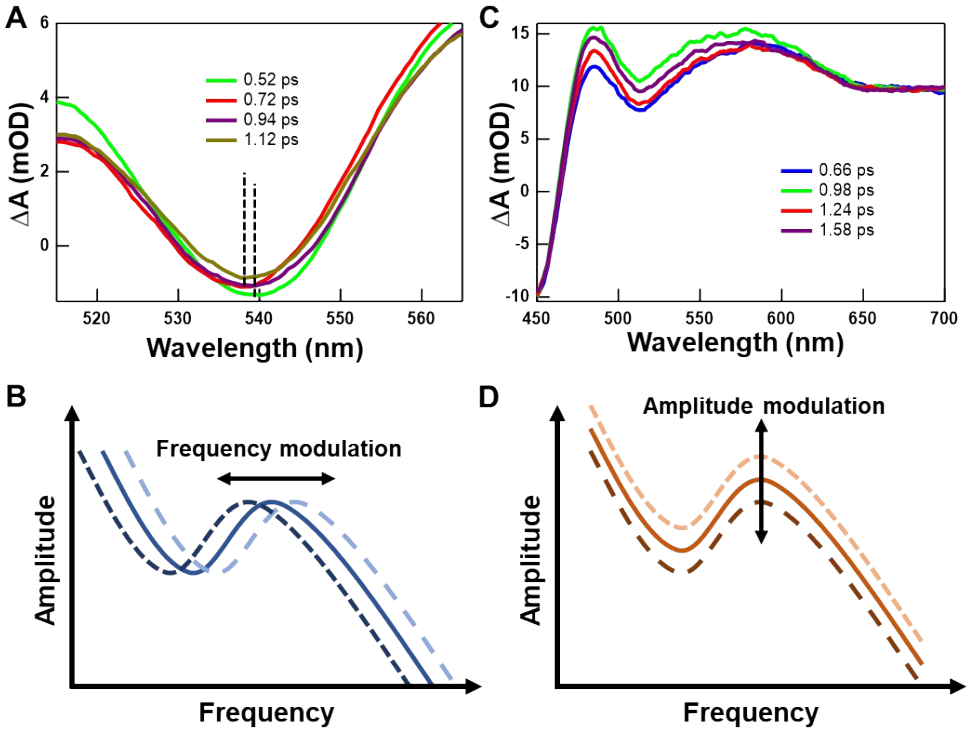

Figure S16. (A) The GSB position of Ag_{44} at different time delay. (B) The schematic diagram of frequency modulated oscillations. (C) The TA spectra of Ag_{29} at different time delay. (D) The schematic diagram of amplitude modulated oscillations.

References.

1. Humphrey, W.; Dalke, A.; Schulten, K. Vmd: Visual Molecular Dynamics. *J. Mol. Graph.* **1996**, *14*, 33-38.

2. Zhang, W.; Kong, J.; Li, Y.; Kuang, Z.; Wang, H.; Zhou, M. Coherent Vibrational Dynamics of Au144(SR)60 Nanoclusters. *Chem. Sci.* **2022**, *13*, 8124-8130.

3. Merrick, J. P.; Moran, D.; Radom, L. An Evaluation of Harmonic Vibrational Frequency Scale Factors. *J. Phys. Chem. A* **2007**, *111*, 11683-11700.

4. Russell, J., Nist 101. Computational Chemistry Comparison and Benchmark Database. CCCBDBDComputational Chemistry Comparison and Benchmark Database: 1999.